Journal of Catalysis 282 (2011) 249–257

Contents lists available at ScienceDirect

Journal of Catalysis

journal homepage: www.elsevier.com/locate/jcat

Experimental and computational investigations of sulfur-resistant bimetallic catalysts for reforming of biomass gasification products

Meghana Rangan [a], Matthew M. Yung [b], J. William Medlin [a,*]

[a] Department of Chemical and Biological Engineering, University of Colorado, Boulder, CO 80309, United States
[b] National Bioenergy Center, National Renewable Energy Laboratory, Golden, CO 80401, United States

ARTICLE INFO

Article history:
Received 2 September 2010
Revised 12 May 2011
Accepted 13 June 2011
Available online 29 July 2011

Keywords:
Steam reforming
Tar
Ni catalyst
Sulfur poisoning
Biomass
Thermochemical conversion

ABSTRACT

A combination of density functional theory (DFT) calculations and experimental studies of supported catalysts was used to identify H_2S-resistant biomass gasification product reforming catalysts. DFT calculations were used to search for bimetallic, nickel-based (1 1 1) surfaces with lower sulfur adsorption energies and enhanced ethylene adsorption energies. These metrics were used as predictors for H_2S resistance and activity toward steam reforming of ethylene, respectively. Relative to Ni, DFT studies found that the Ni/Sn surface alloy exhibited enhanced sulfur resistance and the Ni/Ru system exhibited an improved ethylene binding energy with a small increase in sulfur binding energy. A series of supported bimetallic nickel catalysts was prepared and screened under model ethylene reforming conditions and simulated biomass tar reforming conditions. The observed experimental trends in activity were consistent with theoretical predictions, with observed reforming activities in the order Ni/Ru > Ni > Ni/Sn. Interestingly, Ni/Ru showed a high level of resistance to sulfur poisoning compared with Ni. This sulfur resistance can be partly explained by trends in sulfur versus ethylene binding energy at different types of sites across the bimetallic surface.

1. Introduction

Biofuels produced from biomass gasification hold great promise as a domestic, renewable, and sustainable energy resource [1]. Design of improved heterogeneous catalysts for the complex systems of reactions in gasification and downstream processes is a challenging objective. For example, the reforming of "tar" produced from gasification of biomass involves a relatively large number of reactions, summarized in Scheme 1 [2–4]. Biomass tars, though variable in composition, generally consist of a range of organic hydrocarbons, including paraffins, olefins, and aromatics [2,5]. This mixture of hydrocarbons often gets deposited on surfaces in filters, heat exchangers, engines, and piping, where they reduce component performance and increase maintenance requirements. Thus, hydrocarbon cracking and reforming can increase the efficiency of the biomass thermochemical conversion by reducing maintenance costs and also increasing carbon efficiency through conversion of tars and hydrocarbons into usable syngas [6].

Supported nickel has been shown to have high catalytic activity for steam reforming of the hydrocarbons produced during biomass gasification [5,7,8]. However, a major issue in the long-term stability and activity of the catalyst is its poor resistance toward deactivation by small levels (typically 50–500 ppm) of sulfur-containing compounds present in the process feed stream [2,9]. Sulfur is known to bind very strongly on the active Ni surface, blocking sites required for the reforming reaction [10]. In some systems, sulfur has also been associated with significant metal restructuring and bulk sulfide formation, which lowers the long-term catalyst stability and regenerability [11,12]. Trace amounts of H_2S present in biomass generated syngas streams are enough to deactivate the catalyst. There is a significant need to develop catalysts that maintain high activity for reforming of biomass gasification products in the presence of sulfur-containing compounds, especially H_2S [10–13]. However, the complexity of the surface reactions involved suggests that first-principles design of such catalysts will be difficult. A simple design approach would be attractive.

In this contribution, we explore the use of simple metrics for design of an improved catalyst for the apparently complex tar reforming process. This approach involves two levels of approximation. The first approximation is that the reaction rate of a single hydrocarbon, ethylene, will correlate with the rates of other hydrocarbons, enabling hydrocarbon reforming catalysts to be designed based on a single reactant. The second approximation is that adsorption energies of ethylene and sulfur will correlate with ethylene reforming activity and sulfur resistance, respectively. Although the binding energy of sulfur is in fact expected to be the key metric determining sulfur resistance, the reforming of ethylene involves multiple surface-catalyzed steps including several surface intermediates. The use of the ethylene binding energy as

* Corresponding author.
E-mail address: will.medlin@colorado.edu (J. William Medlin).

0021-9517/$ - see front matter © 2011 Elsevier Inc. All rights reserved.
doi:10.1016/j.jcat.2011.06.009

$$C_nH_m + nH_2O \rightarrow nCO + (m/2 + n)H_2 \quad \text{[steam reforming]}$$

$$nCO_2 + C_nH_m \rightarrow 2nCO + (m/2)H_2 \quad \text{[CO}_2\text{ (dry) reforming]}$$

$$CO + H_2O \leftrightarrow CO_2 + H_2 \quad \text{[water-gas shift]}$$

Scheme 1. Steam reforming of tar.

a metric for the catalyst activity toward ethylene steam reforming thus assumes that a Bronsted–Evans–Polanyi (BEP) relationship exists for the reaction, as has been shown for numerous other reactions where adsorption energies of simple adsorbates are used to guide design [14,15]. This study focused on whether such assumptions could be used to guide catalyst design for a simulated hydrocarbon reforming system. In line with reports from previous researchers indicating that steam is not involved in the kinetically relevant reforming steps, we have also neglected the role of H_2O in the model [16–18]. As described below, although the use of these metrics yielded a catalyst composition with improved activity and sulfur resistance, the mechanism for sulfur resistance is likely more complex than that implied by the simple design approach.

Because many commercial grade catalysts employ Ni as the active component, bimetallic compositions incorporating Ni were investigated for this study [5,8,19]. The use of surface alloys, bulk alloys, and other bimetallic structures has yielded improvements in many catalytic processes, and in several cases, these have been aided by a computational design approach [20,21]. It has been shown, for example, that the carbon resistance of some Ni-containing alloys (such as NiSn) is far better than that of monometallic Ni. On these surface alloys, the oxidation of carbon has a lower kinetic barrier as compared to C–C bond formation [22,23]. Studies by Rodriguez et al. show that the presence of Sn in a Pt/Sn catalyst minimizes the negative effects of sulfur poisoning [24]. Our objective was to identify a Ni-containing bimetallic that is resistant to sulfur relative to monometallic Ni.

2. Methods

2.1. Theoretical methods

H_2S adsorption and decomposition, as well as ethylene adsorption on the various surfaces, were studied using density functional theory (DFT) calculations performed using the Vienna Ab-initio Simulation Package (VASP) [25,26]. The Kohn–Sham one electron valence states were expanded in a plane wave basis set using the projector augmented wave (PAW) method [27]. A cutoff energy of 350 eV was used in the expansion of the basis set.

A periodic supercell was used to model the Ni(1 1 1) and bimetallic Ni surfaces. In order to determine the equilibrium lattice constant, the bulk Ni or bimetallic Ni was geometrically optimized with a $11 \times 11 \times 11$ Monkhorst–Pack *k*-point mesh to obtain the lowest energy lattice constant [28]. The surface calculations were performed on slabs with a thickness of four atomic layers with at least 10 Å vacuum in the surface normal direction. Previous studies have indicated that a slab with four layers has sufficient thickness to accurately predict H_2S decomposition and coking reaction energies and trends on bimetallic surfaces [23,29,30]. Spin polarization was included in these calculations. It has been reported that H_2S decomposes on single crystal Ni surfaces to form surface S and H for coverages less than 0.5 ML [31,32]. Therefore, as a base case, we used 2×2 unit cells for the surface calculations and examined an adsorbate coverage of 0.25 ML. In all the calculations performed, the top two layers of the slab were relaxed and the Brillouin zone was sampled using a $7 \times 7 \times 1$ Monkhorst–Pack *k*-point mesh [28].

The most stable geometrical configuration was obtained by placing the adsorbate in atop, bridge, fcc hollow, and hcp hollow sites and identifying the site with the lowest energy. The equations used to calculate the reaction energies are shown in Appendix (A.3).

Previous experimental studies have established that some metals (e.g., Sn) tend to strongly surface segregate to form surface alloys when combined with Ni while others (such as Ru) form a homogeneous alloy with Ni [33,34]. Thus, we used density functional theory (DFT) to study H_2S adsorption and decomposition on three different types of surfaces shown in Fig. 1: a pure monometallic Ni(1 1 1) surface, a surface alloy (e.g., Ni_3Sn/Ni(1 1 1)), and a homogeneous alloy (e.g., Ni_3Ru(1 1 1)). The Ni to second metal ratio in each bimetallic layer of the slab was kept at 3:1. We also investigated H_2S adsorption and decomposition on the surface of an inhomogeneous alloy. The presence of Ru–Ru bonds (as well as some Ni surface atoms that are coordinated to only two rather than three Ru atoms) in the inhomogeneous Ni_3Ru(1 1 1) alloy differentiates it from a homogeneous Ni_3Ru(1 1 1) alloy as shown in Fig. S1 of the supplementary information.

In selected calculations, we studied the adsorption energies for S and C_2H_4 co-adsorbed on Ni_8Ru(1 1 1). For this study, we used 3×3 unit cells and 1/9 ML coverage of C_2H_4 and S on the surface. The calculations were performed on slabs with a thickness of three layers. In the Ni_8Ru(1 1 1) slab, there is one Ru atom in each layer. The adsorption energies reported in this case are the C_2H_4 binding energies on a S-precovered surface as shown in the equation (A.1). We also compared the minimum energy path for H dissociation from C_2H_4 on Ni(1 1 1) and Ni_8Ru(1 1 1) using the nudged elastic band (NEB) method as implemented in VASP [35,36].

In order to study S coverage effects at a fixed metal composition, we investigated 1/16 ML and 1/8ML S adsorbed on $Ni_{12}Ru_4$. We performed these calculations on 4×4 unit cells with three layers. There are 4 Ru atoms in each layer of the $Ni_{12}Ru_4$(1 1 1) slab. We also studied the adsorption of 1/16 ML coverage of S and C_2H_4 co-adsorbed on Ni(1 1 1) and $Ni_{12}Ru_4$(1 1 1). As on Ni_8Ru(1 1 1), the adsorption energies reported in this case are the C_2H_4 binding energies on a S-precovered surface (A.2).

2.2. Catalyst synthesis

Single aqueous solutions were prepared from the appropriate precursors of $Ni(NO_3)_2{\cdot}6H_2O$, $RuCl_3$, and $SnCl_2$ (Aldrich), which were then used to add 6 wt.% Ni and various amounts of Sn or Ru to an α-Al_2O_3 support (Saint Gobain SA 5397) via incipient wetness impregnation. Catalysts were dried at 110 °C for 3 h and then ramped at 10 °C/min and calcined in air at 650 °C for 5 h. Catalyst naming corresponds to the molar ratio between Ni and the promoter (e.g., $Ru_{0.33}Ni/\alpha$-Al_2O_3 corresponds to 6%Ni/α-Al_2O_3 with a 0.33:1 Ru/Ni molar ratio).

2.3. Catalyst characterization

Temperature-programmed reduction (TPR) was made on 70–100 mg of sample using 35 sccm 10%H_2/Ar and ramping from 50 to 850 °C at 10 °C/min, and H_2 consumption was measured using a TCD to reference the reactor inlet stream to the gas at the reactor exit, after being sent through molecular sieves to remove moisture. X-ray diffraction (XRD) scans from 20 to 80° 2Θ were performed on a Scintag diffractometer using a step size of 0.03°. Electron microscopy was conducted using a low vacuum scanning electron microscope (JSM-7401F) at the Nanomaterials Characterization Facility (University of Colorado, Boulder). An Energy Dispersive X-ray Spectrometer (EDS) installed in this microscope was used for local elemental analysis of catalyst samples. Surface charging was eliminated with a special sample bias

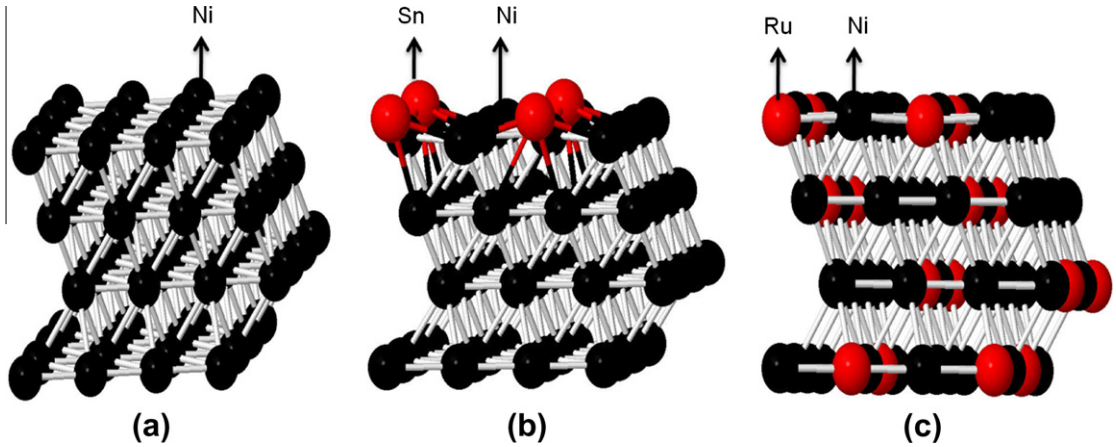

Fig. 1. The figure shows a four-layered model system of: (a) a Ni (1 1 1) slab, (b) a NiSn surface alloy, and (c) a NiRu homogeneous alloy. The Ni atoms are colored black, and the second metal in the bimetallic alloys (i.e., Sn and Ru) are colored red. (For interpretation of the references to color in this figure legend, the reader is referred to the web version of this article.)

voltage option. X-ray absorption fine structure (XAFS) spectroscopy was performed at DuPont-Northwestern-Dow (DND) Collaborative Access Team (CAT) beamline 5-BM-D (BM = bending magnet, http://www.dnd.aps.anl.gov/) at the Advanced Photon Source, Argonne National Laboratory. The XAFS spectra were analyzed using the Athena software package as described previously by Yung et al. [37–39].

2.4. Ethylene and synthetic syngas steam reforming

Catalysts (100 mg) were heated from 25 to 850 °C at 10 °C/min in 10%H_2/N_2, and then held at 850 °C for 1.5 h to pretreat the samples prior to reaction. All flow rates (dry) were 200 sccm in the reaction studies. Catalyst tests lasted 3 h, consisting of (i) 1 h exposure to reaction gases without H_2S, (ii) 1 h exposure to reaction gases with H_2S, and (iii) 1 h exposure to reaction gases without H_2S. Catalysts were examined for ethylene steam reforming (15% C_2H_4, 5 ppm H_2S when included, balance N_2/He + 0.3 mL/min water) and synthetic "syngas" steam reforming (765 ppm benzene, 3.4% C_2H_4, 12.7% CH_4, 21% H_2, 21% CO, 16.9% CO_2, 50 ppm H_2S when included, balance N_2/He + 0.2 mL/min water). These reaction studies were carried out at 850 °C. The gas exiting the reactor was sent to a condenser chilled with water at 4 °C and then through a N_2 membrane dryer to remove moisture before being sent to a Varian micro-GC to measure gas compositions.

3. Results

3.1. Density functional theory

A number of bimetallic compositions were screened using DFT in an attempt to identify promising sulfur-resistant bimetallic compositions that retain high activity—those that show reduced affinity for S-containing adsorbates but favor C_2H_4 adsorption—but most compositions were rejected as unpromising (see Table S1 of the supplementary information). The DFT calculations suggested that, of the bimetallic compositions screened, the NiSn surface alloy has the highest resistance to sulfur while the NiRu homogeneous alloy binds ethylene most strongly. Therefore, the discussion below focuses on NiSn and NiRu.

3.1.1. H_2S adsorption and decomposition

DFT calculations predict that the adsorption and dissociation of H_2S on Ni(1 1 1) are highly favorable as seen in Table 1. The predicted geometries for H_2S and S adsorption on Ni(1 1 1) are in agreement with the geometries observed by Alfonso [40] and Choi et al. [41]. The adsorption and dissociation energies of H_2S on a monometallic Ni(1 1 1) surface, a NiSn surface alloy and a NiRu homogeneous alloy, shown in Table 1, suggest that the Ni_3Sn/Ni(1 1 1) surface alloy is far more sulfur resistant than a monometallic Ni surface. On the Ni_3Sn/Ni(1 1 1) surface alloy, the H_2S adsorption step is endothermic at +0.23 eV and the most favorable adsorption site for S is the hollow site away from the Sn atom. In the case of the Ni_3Ru(1 1 1) slab, H_2S adsorption and dissociation is highly favorable on sites closer to the Ru atom. On the hollow site close to the Ru atom in the Ni_3Ru(1 1 1) surface, the second dissociation step, where SH dissociates to S and H, is approximately equal to that on monometallic Ni(1 1 1). However, on the hollow site closer to the Ni atom, the reaction energy for the second dissociation step is less favorable than on a monometallic Ni surface by almost 0.32 eV. This indicates that S atoms are less likely to bind to the Ni atoms in the presence of Ru at this surface coverage. For reference, we studied H_2S adsorption and decomposition on a pure Ru surface. On Ru(0 0 0 1), we observed that H_2S adsorption and decomposition are exothermic but to a lesser degree than on both monometallic Ni and Ni_3Ru (Table S1). The computed geometries for S adsorption on Ni(1 1 1), Ni_3Sn/Ni(1 1 1), and Ni_3Ru(1 1 1) are shown in Figs. S2, S3, and S4 of the supplementary information.

3.1.2. Ethylene adsorption

As observed previously by other researchers, we found that C_2H_4 binds atop Ni atoms on the Ni(1 1 1) surface with an adsorption energy of −0.70 eV [42]. The DFT results, shown in Table 1, suggest that C_2H_4, the probe molecule for steam reforming activity, does not bind strongly to Ni_3Sn/Ni(1 1 1), with an adsorption energy of just −0.02 eV. As with adsorption of the sulfuric species, ethylene preferentially binds above Ni atoms rather than Sn atoms. However, C_2H_4 binds on the Ni_3Ru(1 1 1) surface more favorably than on the monometallic Ni surface. We observed that the C_2H_4 binding energy is −1.37 eV on top of the Ru atom and −0.51 eV on top of the Ni atom in the Ni_3Ru alloy. This implies that ethylene binding is more favorable compared with that of Ni(1 1 1) atop the Ru atoms in the Ni_3Ru alloy. The ethylene adsorption energy on Ru(0 0 0 1) (Table S1 of the supplementary information) is −0.77 eV, which is very similar to the ethylene adsorption energy on Ni(1 1 1) but considerably lower than that on the Ru atoms of Ni_3Ru(1 1 1). The predicted geometries for C_2H_4 adsorption on Ni(1 1 1), Ni_3Sn/Ni(1 1 1) and Ni_3Ru(1 1 1) are shown in Figs. S2, S3, and S4 of the supplementary information.

Table 1
Reaction energy values for H_2S adsorption and dissociation and ethylene binding on Ni(1 1 1), Ni_3Sn/Ni(1 1 1), and Ni_3Ru(1 1 1).

Slab	H_2S adsorption step[a] (eV)	First dissociation step[b] (eV)	Second dissociation step[c] (eV)	C_2H_4 adsorption (eV)
Ni(1 1 1)	−0.54	−0.79	−1.91	−0.70
Ni_3Sn/ Ni(1 1 1)	+0.23	−0.19	−0.31	−0.02
Ni_3Ru(1 1 1)[d]				
Ru atom	−0.81	−0.76	−1.89	−1.37
Ni atom	−0.54	−1.04	−1.59	−0.51

[a] Adsorption step: $H_2S_{(gas)} \rightarrow H_2S_{(ads)}$.
[b] First dissociation step: $H_2S_{(ads)} \rightarrow SH_{(ads)} + H_{(ads)}$.
[c] Second dissociation step: $SH_{(ads)} \rightarrow S_{(ads)} + H_{(ads)}$.
[d] On Ni_3Ru(1 1 1), energies are reported for adsorption on sites close to the Ru atom and sites close to the Ni atom.

3.1.3. S and C_2H_4 co-adsorbed on Ni(1 1 1), Ni_8Ru(1 1 1) and $Ni_{12}Ru_4$(1 1 1)

Based on the calculations of the adsorption energies of simple sulfuric adsorbates and ethylene, one might expect that the C_2H_4 binding (and subsequent reaction) in the presence of S might be stronger on the Ni_3Ru(1 1 1) surface compared with that of Ni(1 1 1). Sulfur adsorption is less favorable, by 0.39 eV, on the Ni sites than on the Ru sites in the Ni_3Ru(1 1 1) surface. Ethylene adsorption atop the Ru atom in Ni_3Ru(1 1 1) is more favorable as compared to that on the Ni atom by almost 0.81 eV. This suggests a possible situation in which the sulfur poison accumulates on Ni but the C_2H_4 is still reactive on Ru sites. (This conjecture, in fact, was used to guide the experiments described below.) However, it is useful to explicitly consider the co-adsorption of C_2H_4 and S using DFT. We studied the reaction energies upon co-adsorbing S and C_2H_4 on the Ni(1 1 1) and Ni_8Ru(1 1 1) surfaces with 3×3 unit cells (Fig. 2). The energies reported in this section are energies for C_2H_4 adsorption on the energy-minimized 1/9ML S-precovered surface. We observed that an increase in distance between the C_2H_4 and S adsorption sites led to an increase in the exothermicity of C_2H_4 adsorption on the S-precovered surface. Therefore, the energies discussed in this section are for geometries where C_2H_4 and S are as far apart as possible on a 3×3 unit cell. On the Ni(1 1 1) surface, the adsorption energy for C_2H_4 to adsorb on the S-covered surface is −0.71 eV, i.e., essentially the same as on the clean surface. On the Ni_8Ru(1 1 1) surface, we probed two likely geometries for the co-adsorption of S and C_2H_4: (i) S adsorbed on the hollow site near the Ru atom, with C_2H_4 adsorbed atop a Ni atom remote from the Ru, and (ii) S adsorbed on the hollow site composed of Ni atoms, with C_2H_4 adsorbed atop a Ru atom. Our results indicate that the C_2H_4 adsorption energy in the first case is −0.40 eV. The adsorption energy when C_2H_4 is adsorbed atop a Ru atom, with S adsorbed on the hollow site composed of Ni atoms, is far more favorable at −1.04 eV, indicating that C_2H_4 adsorbs more strongly on the S-covered Ni_8Ru(1 1 1) surface than on Ni(1 1 1). This trend is similar to that conjectured above and suggests a complex role of the bimetallic. The dependence of adsorption energy on positions of the co-adsorbates and its possible influence on catalysis are discussed below. However, these results suggest that NiRu catalysts exhibit stronger ethylene binding in the presence of sulfur, and such catalysts were therefore identified as promising candidates for experimental study.

On a 1/16ML S-precovered Ni(1 1 1) slab consisting of 4×4 unit cells and three layers, the ethylene binding energy is −0.88 eV. On the 1/16 ML S-precovered $Ni_{12}Ru_4$(1 1 1) slab, with S adsorbed on the Ru hollow site, C_2H_4 adsorbs on top of the Ni atom with an energy of −0.71 eV. C_2H_4 adsorbs more favorably atop the Ru atom with an adsorption energy of −0.89 eV. The sulfur in this case is adsorbed on the Ni hollow site, away from the Ru atom. These DFT results indicate that the binding energy of C_2H_4 on a 1/16 ML S-precovered $Ni_{12}Ru_4$ surface is closer to that on the 1/16 ML S-precovered Ni(1 1 1). This implies that C_2H_4 adsorption on an S-precovered NiRu surface is more favorable at a lower concentration of Ru in the bimetallic alloy (i.e., Ni_8Ru), where the Ru atoms are more dilute in the bimetallic. However, these calculations only probe adsorption of a single S/C_2H_4 pair per Ru atom, and more dilute Ru bimetallics also present fewer Ru sites for reaction.

3.2. Catalyst characterization

To test the trends in reactivity suggested in DFT, bimetallic NiRu and NiSn catalysts were synthesized, characterized, and evaluated. Fig. 3 shows the XRD patterns for the reduced and post-reaction Ni-only, $Ru_{0.33}Ni$, and $Sn_{0.1}Ni$ catalysts, as well as the unloaded α-Al_2O_3 support. Cubic nickel (PDF# 65-2865) has reflections at 44.5° and 51.8° for the (1 1 1) and (2 0 0) planes, respectively, which correspond to a lattice spacing of 3.52 Å. The lattice spacing for the reduced and post-reaction Ni-only catalysts was calculated as 3.52 Å using the (1 1 1) and (2 0 0) reflections, showing good agreement with the reference cubic nickel. As compared to the Ni-only catalyst, the $Ru_{0.33}Ni$ and $Sn_{0.1}Ni$ catalysts had (1 1 1) and (2 0 0) reflections shifted to lower 2θ values, indicating larger lattice parameters. The lattice parameter for $Ru_{0.33}Ni$ was calculated as 3.53 Å, and this expansion is expected because Ru has a larger lattice constant than Ni. The lattice parameter for the $Sn_{0.1}Ni$ catalyst was found to be 3.58 Å. We used DFT calculations to determine that the Ni–Ni interatomic distance is 2.49 Å in the Ni(1 1 1) surface and 2.55 Å in Ni_3Ru(1 1 1). The Ni–Ru distance in Ni_3Ru(1 1 1) is also 2.55 Å. This shift of the XRD reflections of the $Ru_{0.33}Ni$ catalysts is consistent with the interaction of Ru with Ni to form bimetallic

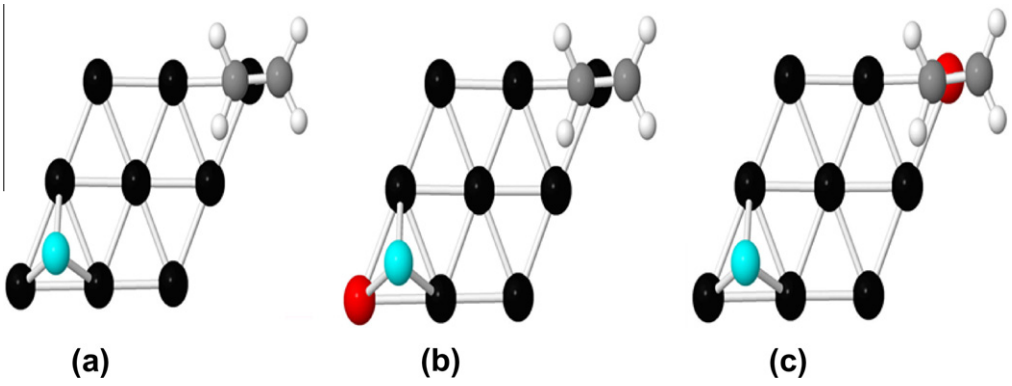

Fig. 2. The figure shows S and C_2H_4 co-adsorbed on: (a) Ni(1 1 1) and (b) Ni_8Ru(1 1 1), with ethylene adsorbed atop the Ni atom and (c) Ni_8Ru(1 1 1) with ethylene adsorbed atop the Ru atom. The black, red, white, gray, and light blue atoms represent Ni, Ru, S, C, and H, respectively. This figure shows only the top-most layer of the three-layer slab. (For interpretation of the references to color in this figure legend, the reader is referred to the web version of this article.)

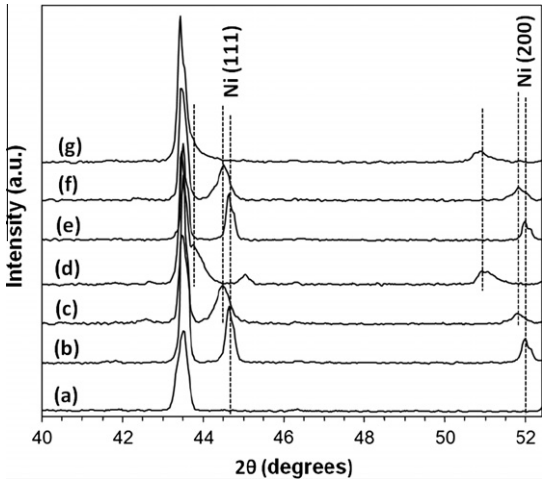

Fig. 3. XRD patterns of: (a) α-Al_2O_3, (b) reduced Ni-only, (c) reduced $Ru_{0.33}Ni$, (d) reduced $Sn_{0.1}Ni$, (e) post-reaction Ni-only, (f) post-reaction $Ru_{0.33}Ni$, and (g) post-reaction $Sn_{0.1}Ni$.

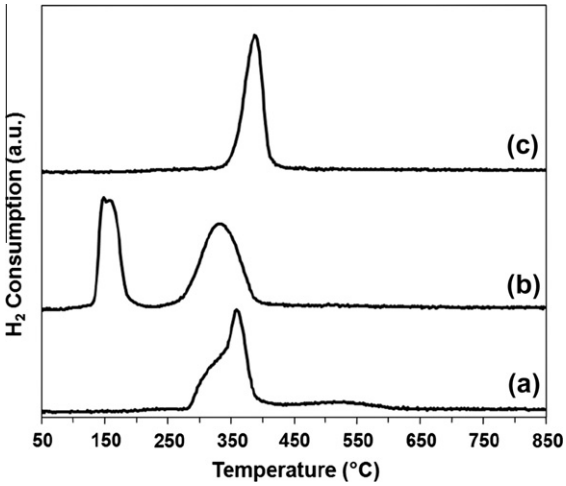

Fig. 4. Characterization via TPR on 6%Ni/α-Al_2O_3 catalysts with various loadings of Ru and Sn: (a) Ni-only, (b) $Ru_{0.33}Ni$, and (c) $Sn_{0.1}Ni$.

crystallites in which both metals are incorporated. As discussed below, the apparent mixing of metals in the reduced catalysts differs somewhat from the situation in the oxidized (pre-reduced) samples, where for example separate oxide phases associated with the Ni and Ru components of the bimetallic are observed (see Fig. S5 of the supplementary information).

Although previous work and the XRD results presented above indicate that the active surface of Ni-based catalysts is metallic under reaction conditions [19], the room-temperature state of the catalyst following calcination is an oxide. TPR studies of the oxidized catalyst can be used to gain insights into its physical structure. The TPR profiles of the catalysts are shown in Fig. 4. The Ni-only sample shows a broad reduction peak from 285 to 400 °C. Comparison of the TPR profiles between the Ni-only and $Ru_{0.33}Ni$ samples shows an increase in the reducibility of Ni^{2+} (NiO) when Ru is added, as indicated by shift to lower reduction temperature, which has been previously observed [43,44] and suggests a significant interaction between Ru and Ni even in the oxidized form of the catalyst. The $Ru_{0.33}Ni$ catalyst shows a low-temperature reduction feature, which can be attributed to RuO_2 particles [45]. While the distinct RuO_2 reduction feature likely indicates some segregation of the oxide particles, the shift to lower NiO reduction temperature on the $Ru_{0.33}Ni$ catalysts can be attributed to RuO_2 in intimate contact with NiO, leading to a reduction of both oxides to form bimetallic Ni–Ru particles [45]. The addition of Sn to Ni/Al_2O_3 led to a narrowing of the Ni^{2+} reduction peak. Sn is known to surface segregate [22], which could lead to stronger interaction between Ni and the Al_2O_3 support, resulting in a decreased contribution of the low-temperature NiO shoulder as compared to the Ni-only catalyst.

Further evidence for the bimetallic nature of the catalysts can be gained from scanning electron microscopy (SEM) and extended X-ray absorption fine structure (EXAFS). SEM images coupled with elemental analysis of the NiRu bimetallic catalysts indicate the bimetallic nature of the supported particles, with Ni and Ru intensity observed in similar locations on line scans. (See, for example, Fig. S6.) Both monometallic and bimetallic catalysts have a broad particle size distribution extending into the micrometer-size range. Fits obtained from analyzing the Ni-edge extended X-ray absorption fine structure (EXAFS) spectra (Fig. S7) of reduced Ni/Al_2O_3 (one shell fit) and reduced $Ru_{0.33}Ni/Al_2O_3$ (two shells fit) indicate that Ni is less coordinated to other Ni atoms in the $Ru_{0.33}Ni/\alpha$-Al_2O_3 as compared to that in Ni/α-Al_2O_3. This decrease in the Ni–Ni coordination number from 8.0 to 5.5 can be attributed to the formation of Ni–Ru bonds in $Ru_{0.33}Ni/\alpha$-Al_2O_3.

3.3. Steam reforming

Ethylene steam reforming results are shown in Fig. 5. Before H_2S was introduced, the trend in ethylene reforming activity was $Ru_{0.33}Ni > Ni > Sn_{0.1}Ni$. The introduction of H_2S led to lower C_2H_4 conversion on all catalysts. Upon removal of H_2S, the activity of the $Sn_{0.1}Ni$ catalyst returned to nearly the same level as prior to H_2S exposure, suggesting that the loss of activity in the presence of H_2S was primarily due to competitive adsorption. On the other catalysts, the partial restoration of activity following removal of H_2S suggests that H_2S caused a decrease in C_2H_4 conversion due to both competitive adsorption and poisoning. The poisoning effect on the $Ru_{0.33}Ni$ catalyst appears to be much less significant than on the Ni catalyst, and the reaction rate in the presence of sulfur is clearly much higher. The similar activity of the $Sn_{0.1}Ni$ catalysts before and after exposure to H_2S, which is nearly the same as the sulfided Ni/Al_2O_3 catalyst, may be explained by Sn adsorption onto the sites that would be poisoned by sulfur, likely undercoordinated Ni step and edge sites, which are also highly active for steam reforming and water–gas shift reactions [46].

The activity of the $Ru_{0.33}Ni$ sample after removal of H_2S was much higher than for the Ni and $Sn_{0.1}Ni$ catalysts. The addition of Ru to Ni catalysts has been shown to increase Ni reducibility and catalyst activity [47], indicating different effects between Ru and

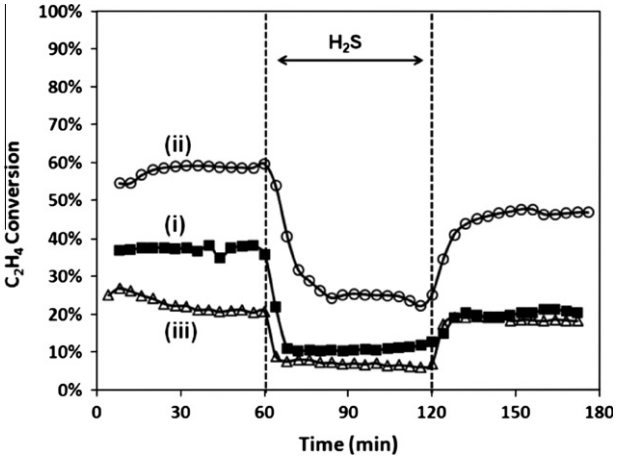

Fig. 5. Activity measurements on 6%Ni/α-Al_2O_3 catalysts with various loadings of Ru and Sn via ethylene steam reforming: (i) Ni-only (shaded squares), (ii) $Ru_{0.33}Ni$ (circles), and (iii) $Sn_{0.1}Ni$ (triangles). These reaction studies were carried out at 850 °C.

Sn for promotion of Ni catalysts. Separate experiments (see Fig. S8 of the supplementary information) using a catalyst with equivalent loadings of Ru but no Ni show reduced activity before introduction of sulfur and very low activity during H_2S exposure. Since the catalysts were not completely saturated with sulfur, these catalysts are not necessarily tolerant to sulfur but are capable of retaining activity in the presence of small amounts of sulfur. So while it is difficult to get uniform H_2S exposure [48], general trends indicate that $Ru_{0.33}Ni$ and $Sn_{0.1}Ni$ show more resistance to sulfur than the Ni catalyst.

The catalysts were subsequently tested in more realistic conditions with multiple tar components to simulate tar reforming of biomass-derived syngas. The CH_4 and C_2H_4 conversion during these experiments is shown in Fig. 6a and b. The relative order of activities for the catalysts is the same as was observed during the C_2H_4 steam reforming experiments. Although the low levels of benzene in the synthetic tar feed resulted in low signal-to-noise in the benzene product signal, the same relative activity order of $Ni_3Ru > Ni > Ni_{10}Sn$ was also observed for the conversion of benzene before and after H_2S exposure (data not shown). At the end of the 180-min experiment (i.e., after H_2S exposure and removal), the exit benzene concentration using the Ni_3Ru was approximately 60% (±10%) lower than that from the pure Ni catalyst, indicating significantly enhanced reactivity on the bimetallic. Following the removal of H_2S from the reactant stream, the conversions of methane, ethylene, and benzene steadily increased for all the samples, indicating in a H_2S-free syngas stream, regeneration of some of the sulfur-poisoned sites may be achieved, likely due to the presence of oxidizing (H_2O) and reducing (CO, H_2) agents.

Although the results reported above were for catalysts having the specific compositions $Sn_{0.1}Ni$ and $Ru_{0.33}Ni$, catalysts having compositions of $Sn_{0.01}Ni$ and $Ru_{0.1}Ni$ were prepared, characterized, and screened and found to follow similar trends. The catalyst with the much lower Ru content was found to have slightly lower activity before and after H_2S exposure, but was still clearly superior to the Ni-only catalyst. (See Fig. S9 of the supporting information.) The improved activity and sulfur resistance of bimetallic NiRu catalysts under both model ethylene reforming and more realistic syngas reforming conditions suggest a bimetallic effect that may be general to this class of reactions. Although this effect is consistent with the enhanced binding of C_2H_4 on both clean and S-precovered $Ni_3Ru(1\,1\,1)$ surfaces (see above), the mechanism for the bimetallic effect may be complex, as discussed below.

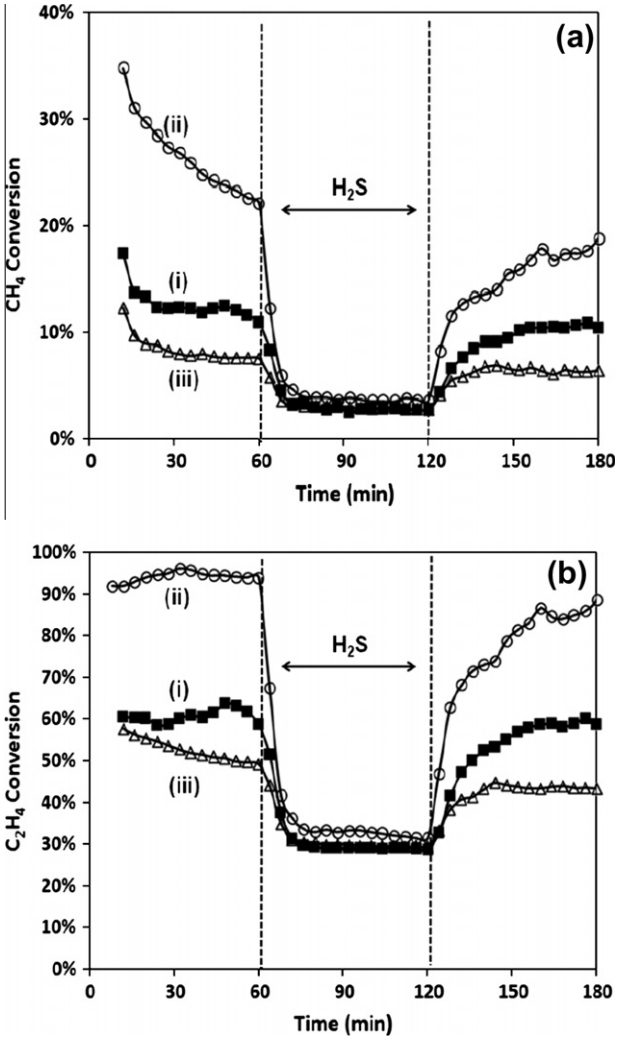

Fig. 6. Conversion plots for: (a) methane and (b) ethylene on 6%Ni/α-Al_2O_3 catalysts with various loadings of Ru and Sn via synthetic syngas steam reforming: (i) Ni-only (shaded squares), (ii) $Ru_{0.33}Ni$ (circles), and (iii) $Sn_{0.1}Ni$ (triangles). These reaction studies were carried out at 850 °C.

4. Discussion

DFT calculations indicate that C_2H_4 does not bind strongly on the NiSn surface alloy. These observations were consistent with the steam reforming experiments that showed low conversions on NiSn catalysts for the steam reforming of both C_2H_4 and synthetic tars. The NiSn surface alloy recovered activity on the removal of H_2S thereby indicating high resistance to sulfur. This is again in agreement with our DFT calculations that indicate weak binding of S on this surface. DFT results suggest that the NiRu homogeneous alloy binds C_2H_4 more strongly than either the Ni(1 1 1) or the Ru(0 0 0 1) slab. This is consistent with the experimental results which indicate that C_2H_4 conversion is higher on NiRu than on either Ni-only or Ru-only catalysts. Mechanisms for poisoning resistance on NiSn bimetallics have already been discussed in detail by previous researchers [22,23]. Therefore, the bulk of this discussion will be devoted toward understanding the effects observed in experiments and calculations on NiRu bimetallics.

The remainder of this section explores connections between the DFT calculations and experimental results described above to identify explanations for the improved reforming activity, both in the absence and in the presence of H_2S, for bimetallic NiRu catalysts compared to Ni. This section is organized as follows. First, we explore the extent to which the model DFT surfaces accurately simulate the relevant surfaces in the experimental studies. Second, we describe possible reasons for the observed trends in DFT results for sulfur and ethylene adsorption. Third, we discuss the extent to which the ethylene adsorption energy may serve as a metric for ethylene steam reforming activity, and furthermore, how considering the adsorption energy in the presence of sulfur may predict activity during sulfur exposure. Finally, we explore the extent to which ethylene steam reforming activity would be expected to correlate with the reactivity of other tar components, such as methane and aromatics.

First, we consider comparisons between the structures modeled in DFT calculations and metal surfaces exposed during catalysis. One approximation is that a closely packed (1 1 1) surface was used for computational studies. This approximation seems reasonable, as the size of the metal crystallites was quite large (see Fig. S6), leading to an expected abundance of (1 1 1) planes on metallic particles. As a partial test of the structure sensitivity of our results, we also studied S and C_2H_4 adsorption on the more open (1 0 0) plane of Ni and Ni_3Ru. The reaction energy for complete decomposition of H_2S was computed to be at −3.46 eV on Ni(1 0 0) (compared to −3.24 eV on Ni(1 1 1)) while the computed ethylene adsorption energies on the two surfaces were computed

to be identical at −0.70 eV. Likewise, S and C_2H_4 adsorption energies on Ni_3Ru(1 0 0) are comparable with those on Ni_3Ru(1 1 1) (−3.42 eV versus −3.46 eV for H_2S decomposition on Ni_3Ru(1 0 0) and Ni_3Ru(1 1 1), and −1.21 eV versus −1.31 eV for ethylene adsorption on those surfaces, respectively). Moreover, the overall trend of Ru addition promoting ethylene adsorption to a greater extent than sulfur adsorption is retained for the (1 0 0) surface.

More difficult is the issue of determining the detailed structure of the bimetallic NiRu particles. As noted above, there is strong evidence from XRD, TPR, SEM, and EXAFS that Ni and Ru are in intimate contact in the catalysts, but the detailed local structure of the active surface cannot be resolved. We used the DFT to determine the formation energies of four NiRu slabs – homogeneous Ni_3Ru, inhomogeneous Ni_3Ru, Ni/Ni_3Ru (monolayer of Ni on Ni_3Ru), and Ru/Ni_3Ru(monolayer of Ru on Ni_3Ru) – using a formulation described earlier by Nikolla et al. [22]. The formation energies at 0 K are in the following order from most favorable to least favorable: Ni/Ni_3Ru (−2.32 eV) > inhomogeneous Ni_3Ru (−2.26 eV) > homogeneous Ni_3Ru (−1.95) > Ru/Ni_3Ru (−1.32 eV). These calculations are indicative of a slight favorability for the formation of a Ni monolayer on Ni_3Ru(1 1 1) at low temperature. The energies of both H_2S decomposition and C_2H_4 adsorption are lower on Ni/Ni_3Ru(1 1 1) than on Ni_3Ru(1 1 1) at −2.71 eV and −0.93 eV, respectively. Again, these results point to preferential stabilization of adsorbed ethylene over adsorbed sulfur. It is noted that Ni monolayers may be less stable at higher temperatures, where entropy effects become increasingly important and Ni atoms are able to rapidly diffuse into the bulk [49,50]. Furthermore, bimetallic crystallites can undergo dramatic changes to their surface composition under high-temperature reaction conditions, and those changes are difficult to characterize [8,51–59]. The increase in reactivity of Ru/Al_2O_3 catalysts after exposure to H_2S (see Fig. S8) may indicate structural changes to the catalyst. Nevertheless, for a variety of surface models having varying crystal faces, Ru contents, and metal distributions, the presence of Ru in the vicinity of the surface alters ethylene and sulfur adsorption in a manner consistent with experimentally observed effects on reforming activity and sulfur resistance.

The description for the binding of olefins such as C_2H_4 to metals was developed by Dewar, Chatt and Duncanson and is known as the DCD model [60,61]. According to this model, there is a donation of charge from the highest occupied π-orbital in ethylene to the metal and a back donation from the filled metal states to the lowest occupied π^*-orbital [60,61]. The π to π^* excitation energy of ethylene ranges between 3.5 and 3.9 eV which is low enough to be compensated by the formation of two covalent bonds to the surface with the C–C bond lying parallel to the surface. Thus, ethylene is bound to the surface in a di-σ configuration [62]. We also observed that the C–C bond is elongated upon adsorption on Ni(1 1 1) and NiRu(1 1 1) from 1.35 Å to 1.43 Å, which is consistent with previous observations [63]. This implies a partial shift from unsaturated sp^2 hybridization for C_2H_4. Ethylene adsorption is more favorable on the NiRu bimetallic than on either Ni(1 1 1) or Ru(0 0 0 1). The DFT results indicate that C_2H_4 binds more strongly on top of the Ru atom in the NiRu slab. A Ru atom in the Ru(0 0 0 1) slab has a d-band center of −2.63 eV, whereas this value is shifted closer to the Fermi level in the Ni_3Ru(1 1 1) slab by 0.54 eV to −2.09 eV. This shift toward the Fermi level is consistent with C_2H_4 binding more favorably on the Ru atom in the Ni_3Ru(1 1 1) surface than the Ru atom in the Ru(0 0 0 1) surface. On the other hand, the d-band center of the Ni atoms in the bimetallic surface is shifted to −1.63 eV, accounting for the weaker adsorption of both species on the Ni atoms of the bimetallic compared to the pure Ni(1 1 1) surface, which has a d-band center of −1.26 eV.

In order for NiRu bimetallics to confer improved ethylene reactivity in the presence of sulfur in the simple model described here, the adsorption energy of ethylene must increase more than the adsorption energy of sulfur when the Ru is introduced. This is in fact observed to be the case in the calculations described above, indicated by both calculations of the individual adsorbates (S and C_2H_4) and the coadsorption of both species on the same slab. Thus, the strengthening of ethylene adsorption on Ru in the bimetallic is greater than the strengthening of sulfur adsorption. Accounting for this fact requires a more detailed analysis of the density of states than the d-band center model yields. Hyman et al. have observed that the d-band center alone does not quantitatively describe S adsorption on various metal surfaces. The density of states at the Fermi level is often an important factor in determining the strength S adsorption on a metal surface [30]. The density of states for a Ni atom in a Ni(1 1 1) surface, a Ni atom in a Ni_3Ru(1 1 1) surface, a Ru atom in a Ni_3Ru(1 1 1) surface, and a Ru atom in a Ru(0 0 0 1) slab is shown in Fig. S10 of the supplementary information. A Ni atom in a pure Ni surface has a greater density of states near the Fermi level than a Ni atom in the Ni_3Ru(1 1 1) surface. This is apparently consistent with S binding more strongly to the Ni hollow site in a Ni(1 1 1) surface than a Ni hollow site in Ni_3Ru(1 1 1) surface.

The mechanism for improved reactivity suggested above is one in which ethylene binds (and reacts) preferentially on the Ru sites while the sulfuric adsorbates segregate to the Ni atoms. This is somewhat reminiscent of the mechanism proposed by Nilekar et al. in their studies of bimetallics for the oxygen reduction reaction; these investigators found that on $Pt_{0.8}M_{0.2}$/Pd(1 1 1) (M = Rh, Ru and Ir), the easily oxidizable metal atoms attract OH at lower potentials, thereby destabilizing OH on adjacent Pt sites and increasing the activity [64]. However, exploratory calculations for different metal compositions and different types of surface alloys complicate this simple understanding. At a lower Ru concentration (i.e., Ni_8Ru), the preferred S adsorption site is the Ni hollow while at a higher concentration of Ru (i.e., Ni_3Ru), the favored adsorption site for S is the Ru-containing hollow. We also observed that S and C_2H_4 adsorption on a Ni_3Ru surface is sensitive to the local surface conditions, using a simple model to describe inhomogeneous distributions of metal atoms near the surface. Our results indicate that an inhomogeneous slab containing Ru–Ru bonds (see Section 2.1 and Table S1) results in somewhat different binding preferences. Ethylene is found to bind more favorably on both the Ru and Ni atoms (where the Ni atom is undercoordinated to Ru atoms as shown in Fig. S1) than on the Ni(1 1 1) surface. In contrast, the presence of Ru–Ru bonds appears to destabilize sulfur adsorption on both types of sites. While this model inhomogeneous surface would still be predicted to yield improved ethylene reactivity in the presence of sulfur compared to pure Ni, it also indicates that more study is needed to conclusively identify the mechanism for sulfur resistance. That work is underway in our laboratory.

Although these observations provide some explanation of the ethylene and sulfur adsorption energy trends, the extent to which these trends would be expected to correlate with ethylene steam reforming activity in the absence and in the presence of H_2S are less immediately clear. Adsorption energies of various species are commonly used as activity predictors in generating "volcano plots" of catalyst performance [65–70]. Use of adsorption energies as activity metrics is generally based on the assumption that a BEP relation exists for the reaction; that is, the (kinetic) activation energy for a rate-limiting step is linearly proportional to a (thermodynamic) difference in adsorption energies for the adsorbed species. These approaches have recently been used with great success for predicting activation barriers based on adsorption energies for reactions of hydrocarbons [71,72]. In the case of methane reforming reactions on metal surfaces, previous work has identified the initial C–H dissociation step as being rate determining on both supported Ni and Ru catalysts [16,73]. Though bimetallic catalysts have not previously been studied in detail, we have assumed that bimetallic compositions of the Ni and Ru components will

likewise be controlled by hydrocarbon adsorption and subsequent C–H activation. We calculated the minimum energy path for C_2H_3–H dissociation on Ni(1 1 1) and Ni_8Ru(1 1 1) and found that C–H bond breaking is clearly favored on Ni_8Ru(1 1 1) (Fig. S11). The adsorbed ethylene reactant, transition state, and C_2H_3 + H product state are all significantly stabilized on Ni_3Ru, and the barrier to reaction is lower by 0.15 eV. The reaction energy for C–H dissociation is found be more exothermic by approximately 0.1 eV on Ni_8Ru(1 1 1) and by 0.6 eV on Ni_3Ru(1 1 1) compared to Ni(1 1 1), consistent with a reduced C–H dissociation barrier for both surfaces. The stronger adsorption of ethylene—which leads to weakened C–H bonds on the ethylene molecule—and of its reaction product C_2H_3 therefore correlates with a lower barrier for the rate-limiting C–H dissociation on the surface. This analysis assumes that the catalyst systems considered here operate on the "right hand side" of a hypothetical volcano curve, i.e., that they are not limited by the number of vacant sites available for ethylene binding and reaction. For the high-temperature reactions explored here and the relatively weak adsorption energies of ethylene, this assumption appears reasonable. Furthermore, a similar BEP relation would be expected for a sulfur-coated surface, where again stronger binding of ethylene would be correlated with increased reactivity, provided that reactivity is not strongly limited by the density of available sites.

Finally, it is worth exploring the extent to which ethylene reactivity would be expected to correlate with the activity of other hydrocarbons such as methane and benzene. Based on the experimental data, a clear correlation exists; yet, it is not obvious that such a correlation would be expected. However, Studt et al. have previously found that acetylene and ethylene adsorption energies scale with the methyl adsorption energies on the same metals, indicating that key hydrocarbons of interest in tar reforming (in particular methane) follow similar trends in adsorption energies [14], assuming similar rate-limiting steps and similar reactivities [16,74]. Such scaling relations were also observed for CH_x adsorbates with differing numbers of H atoms where it was found that any of the molecules considered scaled approximately with the adsorption energy of the central, C, N, O, or S atom, the scaling constant depending only on x [75]. We examined CH_3 adsorption on Ni(1 1 1) and Ni_3Ru(1 1 1) as CH_4 is known to be one of the most recalcitrant components of tar [76]. The trends observed for methyl adsorption were similar to those seen for C_2H_4 adsorption, i.e., Ru atom in NiRu > Ni > Ni atom in NiRu (Table S1), helping to explain the improved performance of NiRu bimetallic catalysts for reforming of the methane as well as ethylene. One reason for the correlation between ethylene and methyl adsorption energies may be the significant rehybridization of ethylene after adsorption, which causes the C atoms to approach sp^3 hybridization as in methyl. In contrast, the explanation for correlation with aromatic reactivities is less clear. Interactions between benzene and metal surfaces are expected to be strongly influenced by the aromaticity of the adsorbate, which is not captured by the methyl and ethylene models [77]. Thus, reasons for the improved benzene conversion during simulated syngas steam reforming are not clear and for now must simply be noted as an interesting observation.

In closing, it is worth noting that the role of the reactant H_2O was not investigated for this work, though the chemistry of H_2O on Ni surfaces has been widely studied earlier [78–80]. It has been reported that molecular adsorption of H_2O on Ni(1 1 1) is reversible. H_2O exothermically dissociates to H and OH on the threefold neighboring sites of the Ni(1 1 1) surface [78]. Stronger adsorption of these species on NiRu catalysts could lead to a reduced density of active sites through competitive adsorption, though such an effect is not obvious from the experimental results in which steam was in great excess. It has also been suggested that the Ni particles sinter more in the presence of steam, thereby increasing the (1 1 1) planes on the metallic particles [4]. The detailed effects of steam on the surface chemistry reported here are the subject of ongoing investigation and are likely important in a complete understanding of the mechanism.

5. Conclusions

DFT calculations were used to study the adsorption of ethylene and sulfuric compounds on Ni(1 1 1) and various bimetallic surfaces. These calculations indicated that a Ni_3Sn surface alloy significantly destabilized both sulfur and ethylene adsorption, while a Ni_3Ru homogeneous alloy stabilizes both sulfur and ethylene adsorption; however, the adsorption of ethylene is stabilized to a greater degree than the adsorption of sulfur. Based on a simple model in which ethylene and sulfur adsorption energies are assumed to be related to ethylene reforming activity and sulfur resistance, respectively, these calculations suggested that Ni_3Sn surface alloys should exhibit reduced activity but excellent sulfur resistance, while Ni_3Ru homogeneous alloys should show improved activity both in the absence and in the presence of sulfur. The general trends in ethylene reforming activity observed for bimetallic NiSn and NiRu catalysts were found to be in agreement with this simple model. Although perturbations to the DFT calculations indicate that the mechanism for the relative sulfur tolerance of NiRu bimetallics is likely to be complex, the results of this study suggest that a relatively simple design approach may be productive in the selection of new catalysts for complex reactions.

Acknowledgments

Research funding from the National Renewable Energy Laboratory through subcontract KXEA-3-33606-26 and from the US Department of Energy's Biomass Program Contract DE-AC36-99-GO-10337 are gratefully acknowledged. This research utilized the NCSA-Teragrid system and the high-performance computing cluster carbon at Argonne National Laboratory. Portions of this work were performed at the DuPont-Northwestern-Dow Collaborative Access Team (DND-CAT) located at Sector 5 of the Advanced Photon Source (APS). DND-CAT is supported by E.I. DuPont de Nemours & Co., The Dow Chemical Company and the State of Illinois. Use of the APS was supported by the US Department of Energy, Office of Science, Office of Basic Energy Sciences, under contract number DE-AC02-06CH11357. Assistance from the DND-CAT beamline scientists, especially from Qing Ma, and from John Kuhn for data acquisition is greatly appreciated.

Appendix A. Equations used to compute adsorption and reactions energies of different species

$$\Delta E_{C_2H_4} = E_{C_2H_4/1/9MLS-Ni_8Ru} - E_{1/9MLS/Ni_8Ru} - E_{C_2H_4} \quad (A.1)$$

$$\Delta E_{C_2H_4} = E_{C_2H_4/1/16MLS-Ni_{12}Ru_4} - E_{1/16MLS/Ni_{12}Ru_4} - E_{C_2H_4} \quad (A.2)$$

$$\begin{aligned} &H_2S_{(gas)} \rightarrow H_2S_{(ads)} \quad \Delta E_1 = E_{H_2S/slab} - E_{H_2S} - E_{slab} \\ &H_2S_{(ads)} \rightarrow SH_{(ads)} + H_{(ads)} \quad \Delta E_2 = E_{SH/slab} + E_{H/slab} - E_{H_2S/slab} - E_{slab} \\ &SH_{(ads)} \rightarrow S_{(ads)} + H_{(ads)} \quad \Delta E_3 = E_{S/slab} + E_{H/slab} - E_{SH/slab} \\ &C_2H_{4_{(gas)}} \rightarrow C_2H_{4_{(ads)}} \quad \Delta E_4 = E_{C_2H_4/slab} - E_{C_2H_4} - E_{slab} \end{aligned} \quad (A.3)$$

Appendix B. Supplementary material

Supplementary data associated with this article can be found, in the online version, at doi:10.1016/j.jcat.2011.06.009.

References

[1] L.R. Lynd, C.E. Wyman, T.U. Gerngross, Biotechnol. Prog. 15 (1999) 777–793.
[2] M.M. Yung, W.S. Jablonski, K.A. Magrini-Bair, Energy Fuels 23 (2009) 1874–1887.
[3] R.D. Cortright, R.R. Davda, J.A. Dumesic, Nature 418 (2002) 964–967.
[4] J. Sehested, J.A.P. Gelten, I.N. Remediakis, H. Bengaard, J.K. Norskov, J. Catal. 223 (2004) 432–443.
[5] K.A. Magrini-Bair, S. Czernik, R. French, Y.O. Parent, E. Chornet, D.C. Dayton, C. Feik, R. Bain, Appl. Catal. A – Gen. 318 (2007) 199–206.
[6] R.Q. Zhang, R.C. Brown, A. Suby, K. Cummer, Energy Convers. Manage. 45 (2004) 995–1014.
[7] C.A. Bernardo, I. Alstrup, J.R. Rostrupnielsen, J. Catal. 96 (1985) 517–534.
[8] T. Kimura, T. Miyazawa, J. Nishikawa, S. Kado, K. Okumura, T. Miyao, S. Naito, K. Kunimori, K. Tomishige, Appl. Catal. B – Environ. 68 (2006) 160–170.
[9] G.A. Sargent, J.L.R. Chao, G.B. Freeman, Appl. Surf. Sci. 7 (1981) 104–114.
[10] W.T. Owens, N.M. Rodriguez, R.T.K. Baker, Catal. Today 21 (1994) 3–22.
[11] R. Backer, G. Horz, Vacuum 46 (1995) 1101–1104.
[12] A. Kulprathipanja, G.O. Alptekin, J.L. Falconer, J.D. Way, J. Membr. Sci. 254 (2005) 49–62.
[13] J. Sehested, Catal. Today 111 (2006) 103–110.
[14] F. Studt, F. Abild-Pedersen, T. Bligaard, R.Z. Sorensen, C.H. Christensen, J.K. Norskov, Science 320 (2008) 1320–1322.
[15] J. Greeley, J.K. Norskov, J. Phys. Chem. C 113 (2009) 4932–4939.
[16] J.M. Wei, E. Iglesia, J. Catal. 224 (2004) 370–383.
[17] A. Yamaguchi, E. Iglesia, J. Catal. 274 (2010) 52–63.
[18] A. Ishikawa, M. Neurock, E. Iglesia, J. Am. Chem. Soc. 129 (2007) 13201–13212.
[19] M.P. Aznar, J. Corella, J. Delgado, J.Q. Lahoz, Ind. Eng. Chem. Res. 32 (1993) 1–10.
[20] C.H. Christensen, J.K. Norskov, J. Chem. Phys. 128 (2008).
[21] C.J.H. Jacobsen, S. Dahl, B.S. Clausen, S. Bahn, A. Logadottir, J.K. Norskov, J. Am. Chem. Soc. 123 (2001) 8404–8405.
[22] E. Nikolla, J. Schwank, S. Linic, J. Catal. 250 (2007) 85–93.
[23] E. Nikolla, A. Holewinski, J. Schwank, S. Linic, J. Am. Chem. Soc. 128 (2006) 11354–11355.
[24] J.A. Rodriguez, Prog. Surf. Sci. 81 (2006) 141–189.
[25] G. Kresse, J. Hafner, Phys. Rev. B 47 (1993) 558–561.
[26] G. Kresse, J. Furthmuller, Comput. Mater. Sci. 6 (1996) 15–50.
[27] G. Kresse, D. Joubert, Phys. Rev. B 59 (1999) 1758–1775.
[28] H.J. Monkhorst, J.D. Pack, Phys. Rev. B 13 (1976) 5188–5192.
[29] H. Jiang, H. Yang, R. Hawkins, Z. Ring, Catal. Today 125 (2007) 282–290.
[30] M.P. Hyman, B.T. Loveless, J.W. Medlin, Surf. Sci. 601 (2007) 5382–5393.
[31] D.R. Huntley, Surf. Sci. 240 (1990) 24–36.
[32] D.R. Huntley, Surf. Sci. 240 (1990) 13–23.
[33] S.H. Overbury, Y.S. Ku, Phys. Rev. B 46 (1992) 7868–7872.
[34] X. He, L.T. Kong, J.H. Li, X.Y. Li, B.X. Liu, Acta Mater. 54 (2006) 3375–3381.
[35] G. Henkelman, B.P. Uberuaga, H. Jonsson, J. Chem. Phys. 113 (2000) 9901–9904.
[36] G. Henkelman, H. Jonsson, J. Chem. Phys. 113 (2000) 9978–9985.
[37] M.M. Yung, J.N. Kuhn, Langmuir 26 (2010) 16589–16594.
[38] B. Ravel, M. Newville, J. Synchrotron Radiat. 12 (2005) 537–541.
[39] M. Newville, J. Synchrotron Radiat. 8 (2001) 96–100.
[40] D.R. Alfonso, Surf. Sci. 602 (2008) 2758–2768.
[41] Y.M. Choi, C. Compson, M.C. Lin, M.L. Liu, Chem. Phys. Lett. 421 (2006) 179–183.
[42] N.D. Yilmazer, M.F. Fellah, I. Onal, Appl. Surf. Sci. 256 (2010) 5088–5093.
[43] A. Masalska, Catal. Today 137 (2008) 439–445.
[44] A. Masalska, Catal. Lett. 127 (2009) 158–166.
[45] J.M. Rynkowski, T. Paryjczak, M. Lenik, Appl. Catal. A – Gen. 126 (1995) 257–271.
[46] J. Rostrup-Nielsen, J.K. Norskov, Top. Catal. 40 (2006) 45–48.
[47] J.H. Jeong, J.W. Lee, D.J. Seo, Y. Seo, W.L. Yoon, D.K. Lee, D.H. Kim, Appl. Catal. A – Gen. 302 (2006) 151–156.
[48] C.H. Bartholomew, P.K. Agrawal, J.R. Katzer, Adv. Catal. 31 (1982) 135–242.
[49] J.R. Kitchin, N.A. Khan, M.A. Barteau, J.G. Chen, B. Yakshinksiy, T.E. Madey, Surf. Sci. 544 (2003) 295–308.
[50] M.P. Humbert, C.A. Menning, J.G. Chen, J. Catal. 271 (2010) 132–139.
[51] J. Sehested, J.A.P. Gelten, S. Helveg, Appl. Catal. A – Gen. 309 (2006) 237–246.
[52] M. Nurunnabi, Y. Mukainakano, S. Kado, B.T. Li, K. Kunimori, K. Suzuki, K. Fujimoto, K. Tomishige, Appl. Catal. A – Gen. 299 (2006) 145–156.
[53] X.F. Tang, Y.G. Li, X.M. Huang, Y.D. Xu, H.Q. Zhu, J.G. Wang, W.J. Shen, Appl. Catal. B – Environ. 62 (2006) 265–273.
[54] B. Mirkelamoglu, G. Karakas, Appl. Catal. A – Gen. 299 (2006) 84–94.
[55] V.A. Bogdanovskaya, M.R. Tarasevich, L.A. Reznikova, L.N. Kuznetsova, Russ. J. Electrochem. 46 (2010) 1011–1020.
[56] Y.V. Guryev, Ivanova II, V.V. Lunin, W. Gruenert, M.W.E. van den Berg, Appl. Catal. A – Gen. 329 (2007) 16–21.
[57] Y. Mukainakano, B.T. Li, S. Kado, T. Miyazawa, K. Okumura, T. Miyao, S. Naito, K. Kunimori, K. Tomishige, Appl. Catal. A – Gen. 318 (2007) 252–264.
[58] B.T. Li, S. Kado, Y. Mukainakano, T. Miyazawa, T. Miyao, S. Naito, K. Okumura, K. Kunimori, K. Tomishige, J. Catal. 245 (2007) 144–155.
[59] W.K. Jozwiak, M. Nowosielska, J. Rynkowski, Appl. Catal. A – Gen. 280 (2005) 233–244.
[60] M.J.S. Dewar, Bull. Soc. Chim. France 18 (1951) c79.
[61] J. Chatt, L.A. Duncanson, J. Chem. Soc. (1953) 2939–2947.
[62] A. Nilsson, L.G.M. Pettersson, J.K. Nørskov, Chemical Bonding at Surfaces and Interfaces, Elsevier, Amsterdam, 2008.
[63] H. Ostrom, A. Fohlisch, M. Nyberg, M. Weinelt, C. Heske, L.G.M. Pettersson, A. Nilsson, Surf. Sci. 559 (2004) 85–99.
[64] A.U. Nilekar, Y. Xu, J.L. Zhang, M.B. Vukmirovic, K. Sasaki, R.R. Adzic, M. Mavrikakis, Top. Catal. 46 (2007) 276–284.
[65] L.C. Grabow, B. Hvolbaek, J.K. Norskov, Top. Catal. 53 (2010) 298–310.
[66] J.K. Norskov, T. Bligaard, B. Hvolbaek, F. Abild-Pedersen, I. Chorkendorff, C.H. Christensen, Chem. Soc. Rev. 37 (2008) 2163–2171.
[67] T. Bligaard, J.K. Norskov, S. Dahl, J. Matthiesen, C.H. Christensen, J. Sehested, J. Catal. 224 (2004) 206–217.
[68] H. Falsig, T. Bligaard, J. Rass-Hansen, A.L. Kustov, C.H. Christensen, J.K. Norskov, Top. Catal. 45 (2007) 117–120.
[69] S. Dahl, A. Logadottir, C.J.H. Jacobsen, J.K. Norskov, Appl. Catal. A – Gen. 222 (2001) 19–29.
[70] A. Logadottir, T.H. Rod, J.K. Norskov, B. Hammer, S. Dahl, C.J.H. Jacobsen, J. Catal. 197 (2001) 229–231.
[71] D.C. Ford, A.U. Nilekar, Y. Xu, M. Mavrikakis, Surf. Sci. 604 (2010) 1565–1575.
[72] P. Ferrin, D. Simonetti, S. Kandoi, E. Kunkes, J.A. Dumesic, J.K. Norskov, M. Mavrikakis, J. Am. Chem. Soc. 131 (2009) 5809–5815.
[73] J.M. Wei, E. Iglesia, J. Phys. Chem. B 108 (2004) 7253–7262.
[74] M. Zboray, A.T. Bell, E. Iglesia, J. Phys. Chem. C 113 (2009) 12380–12386.
[75] F. Abild-Pedersen, J. Greeley, F. Studt, J. Rossmeisl, T.R. Munter, P.G. Moses, E. Skulason, T. Bligaard, J.K. Norskov, Phys. Rev. Lett. 99 (2007).
[76] M.M. Yung, K.A. Magrini-Bair, Y.O. Parent, D.L. Carpenter, C.J. Feik, K.R. Gaston, M.D. Pomeroy, S.D. Phillips, Catal. Lett. 134 (2010) 242–249.
[77] M. Cruz, J. Carneiro, D.A.G. Aranda, M. Buhl, J. Phys. Chem. C 111 (2007) 11068–11076.
[78] M.L. Ferreira, N.N. Nichio, O.A. Ferretti, J. Mol. Catal. A – Chem. 202 (2003) 197–213.
[79] N. Lakshminarayanan, U.S. Ozkan, Appl. Catal. A – Gen. 393 (2010) 138–145.
[80] C. Pistonesi, A. Juan, B. Irigoyen, N. Amadeo, Appl. Surf. Sci. 253 (2007) 4427–4437.